

A novel approach to atmospheric profiling with a mountain-based or airborne GPS receiver

Cinzia Zuffada, George A. Hajj, E. Robert Kursinski

Jet Propulsion Laboratory, California Institute of Technology, Pasadena

Abstract. The delay induced by the Earth's atmosphere on the Global Positioning System (GPS) signal has been exploited in the last decade for atmospheric remote sensing. Ground-based GPS measurements are traditionally used to derive columnar water vapor content, while space-based GPS measurements, obtained by a receiver in a low-Earth orbit tracking GPS satellites occulting behind the Earth's atmosphere, yield accurate, high-resolution profiles of refractivity, temperature, and water vapor. A GPS receiver on a mountain top or an airplane with a "downward looking" field of view toward the Earth's limb is a novel concept presented here. We describe a generalized ray-tracing inversion scheme where spherical symmetry is assumed for the atmosphere, and the refractivity is modeled as piecewise exponential, with scale height changing from one atmospheric layer to the next. Additional refractivity data, derived from a model, might be introduced above the receiver as an a priori constraint, and are treated as properly weighted additional measurements. The exponential scale heights and a normalizing value of refractivity are retrieved by minimizing, in a least squares sense, the residuals between measured bending angles and refractivity and those calculated on the basis of the exponential model and ray-tracing. As a first validation step, we illustrate results comparing refractivity and temperature profiles obtained by this generalized ray-tracing scheme against those derived via the Abel inversion for the GPS/MET experiment. Additionally, we present results for a hypothetical situation where the receiver is located within the atmosphere at a height of 5 km. For the last case we investigate the accuracy of the retrieval both below and above the receiver at a set of locations in the atmosphere ranging from middle to tropical latitudes. The main objective is that of establishing whether the bending measurements have sufficient strength to allow for retrieval of refractivity below and possibly above the receiver location. Our findings suggest that accurate profiles of refractivity at heights ranging from the Earth's surface to slightly above the receiver location can be derived by GPS data collected from within the atmosphere.

1. Introduction

Radio occultation measurements using the Global Positioning System (GPS) and a receiver in a low-Earth orbit (LEO) have recently been shown to provide accurate profiles of atmospheric refractivity, pressure, water vapor, and temperature with high vertical resolution [e.g., Hajj *et al.*, 1996; Kursinski *et al.*, 1996; Ware *et al.*, 1996; Leroy, 1997; Rocken *et al.*, 1997; Kursinski and Hajj, 1998]. The high accuracy and resolution of atmospheric profiles obtained from GPS occultations, at a relatively low cost, are generating considerable interest in the atmospheric and climate research communities. For instance, several studies have investigated means of assimilating GPS occultation data into numerical weather predictions and the impact these data would have on the models [Eyre, 1994; Zou *et al.*, 1995; Kuo *et al.*, 1998; Zou *et al.*, 1998], while others

examined their climate information contents [Yuan *et al.*, 1993; Kursinski and Hajj, 1998; Leroy, 1998].

While GPS occultation data collected from space have the advantage of being global (one receiver in low-Earth orbit provides about 500 globally distributed occultations per day), the sampling in any particular region is relatively sparse without a large number of orbiting receivers. (For a review of the space-based GPS occultation technique see, for example, Kursinski *et al.* [1997].) By contrast, a receiver located inside the Earth's atmosphere (such as on a mountain top, or an airplane) can be used to provide data over specific areas of interest for the purpose of regional weather and climate studies and atmospheric and coupled ocean/atmospheric process research. A mountain-based or airborne receiver would track any GPS satellite as it sets or rises behind the Earth's limb, therefore collecting data at both negative and positive elevations relative to the receiver's local horizon (Figure 1). We have found that by combining both the negative and the positive elevation data we obtain a high-resolution profile of refractivity below the height of the receiver and extending in some cases to 1 km above the receiver.

Copyright 1999 by the American Geophysical Union.

Paper number 1999JD900766.
0148-0227/99/1999JD900766\$09.00

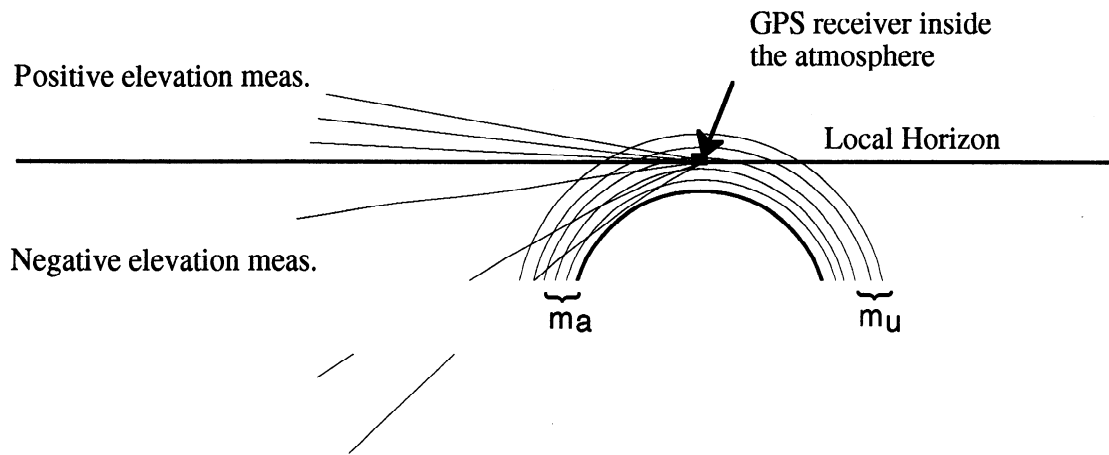


Figure 1. A pictorial view of GPS atmospheric sensing with a receiver inside the atmosphere. The layers of atmosphere below the receiver location are denoted by m_a , and those above the receiver by m_u .

The viewing geometry of a “down looking” GPS receiver located inside the atmosphere can be thought of as a hybrid between the space and the ground viewing geometries; it combines the high vertical profiling capability of space data (at least for heights below the receiver) with the benefit of routinely obtaining a relatively large number of daily profiles in regions of interest. Each occultation will yield a profile of refractivity below the height of the receiver with a diffraction-limited vertical resolution of 150-250 m. Refractivity, in turn, can be converted to a profile of water vapor with an accuracy of about 0.2 g/kg by assuming knowledge of temperature from a numerical weather model (as done by *Kursinski and Hajj* [1998]). A single receiver with a full 360° field of view of the horizon will observe nearly 100 occultations per day scattered within a 200 km radius from the receiver. If the topography of a region allows placement of several receivers, separated by distances of 50-200 km, hundreds of daily occultations can be obtained over that region. This information, when combined with columnar water vapor distribution derived from upward looking ground-based receivers, and possibly moisture information from synthetic aperture radar (SAR) data, is extremely useful for regional weather monitoring and hydrological and boundary layer research.

The goal of this paper is to introduce the limb and down looking GPS receiver concept for the first time, illustrate a ray-tracing inversion scheme suitable for this special sensing geometry, and examine the achievable accuracy, resolution, and the usefulness of this technique.

The ray-tracing-based inversion technique developed here can be considered a generalization of the more traditional “Abel transform” inversion normally used in space-based atmospheric occultation. The challenge associated with inverting data from a down looking airborne receiver is that data collected at positive elevations are only weakly sensitive to the atmospheric vertical structure above it, while obtaining an accurate retrieval below the receiver requires a somewhat accurate knowledge of the refractivity

profile above the receiver. A solution to this problem, which is presented here, is to combine both negative and small-angle positive elevation data in an optimal manner.

The technique presented below can also be used in assimilating GPS occultation data (spacebased or airborne) in numerical weather prediction (NWP). In this context the technique would be relevant to other research on assimilating space-based GPS occultation data into numerical weather models [*Eyre*, 1994; *Gorbunov*, 1996; *Kuo et al.*, 1996; *Zou et al.*, 1998]. Specifically, if retrieved profiles of refractivity were to be assimilated in NWP according to the schemes outlined in the referenced work, the technique described in this paper could be used in the step of inversion of the bending measurements. It is noted that the specific inversion implemented in our work presupposes spherical symmetry. On the other hand, a scheme such as the one suggested by *Eyre* [1994] to account for the horizontal gradients of refractivity could be incorporated into our work in the future.

This paper is structured as follows: In Section 2 we give a brief summary of the GPS occultation technique and the traditional Abel inversion scheme (Section 2.1) and then a detailed description of the new scheme suitable for airborne occultation measurements (Section 2.2), hereinafter referred to as the ray-tracing inversion scheme. In Section 3.1 we compare the ray-tracing inversion scheme to the Abel inversion by applying it on data collected from space with the GPS/MET experiment (GPS/MET is a proof-of-concept experiment which carried a GPS receiver into space for the purpose of atmospheric occultation. It started in 1995 and collected over 2 years worth of occultation data. It is managed by the University Corporation for Atmospheric Research, Boulder, Colorado.) In Section 3.2 we use the new technique in a simulated application where the receiver is assumed to be fixed at 5 km altitude, and both negative and positive elevation bending measurements are collected. Examples at several latitude-longitude positions, representing different climates, are examined to assess the

accuracy and usefulness of this new remote sensing approach. Section 4 presents a summary and conclusions.

2. Inversion Schemes

In a spherically symmetric medium, a signal travels along a curve defined by

$$nr \sin(\phi) = \text{constant} \equiv a, \quad (1)$$

where r is the distance from the origin of symmetry to a point on the ray path, ϕ is the angle between the direction of r and the tangent to the ray path, and n is the index of refraction at r . Equation (1) corresponds to Snell's law in polar coordinates for a spherically symmetric medium, and it is also known as Bouguer's formula. On this basis, a signal traveling in a spherically symmetric medium will bend by an amount [Born and Wolf, 1980]

$$\alpha = -2a \int_a^\infty \frac{1}{n \sqrt{n^2 r^2 - a^2}} \frac{dn}{dr} dr. \quad (2)$$

When the receiver is outside the atmosphere, a corresponds to the asymptote miss distance or impact parameter.

The basic observables of the GPS satellites from which the bending is derived are the L1 (wavelength = 19.0 cm) and L2 (wavelength = 24.4 cm) phase delays. From knowledge of the positions of the transmitter and the receiver and their clocks (which are obtained from other GPS measurements collected simultaneously) the delay due to the intervening media can be isolated. Both L1 and L2 signals are used to calibrate for the dispersive ionosphere, and the extra neutral atmospheric delay is isolated. (For a more detailed discussion of how atmospheric delay is detected, see for example, Hajj et al. [1996].) From knowledge of the atmospheric extra delay as a function of time we can derive the extra atmospheric Doppler which is related to the bending of the signal via the equation

$$\Delta f = \frac{f}{c} (\vec{v}_t \cdot \vec{k}_t - \vec{v}_r \cdot \vec{k}_r - f \vec{v}_t - \vec{v}_r \cdot \vec{k}), \quad (3)$$

where f is the GPS transmitting frequency, c is the speed of light, \vec{v}_t and \vec{v}_r are the transmitter and receiver velocities, respectively, \vec{k}_t and \vec{k}_r are the unit propagation vectors in the direction of the transmitted and received signal, and \vec{k} is the unit vector in the direction of the straight line passing through the transmitter and receiver positions (Figure 2).

From equation (2) and the following equation, which is implied by Bouguer's formula,

$$a = r_t n_t \sin(\theta_t + \delta_t) = r_r n_r \sin(\theta_r + \delta_r), \quad (4)$$

(angles are defined in Figure 2) we can derive the total bending of the signal ($\alpha = \delta_t + \delta_r$) as a function of a . Note that equations (1)-(4) can be applied to GPS data received at either positive or negative elevation. The fundamental function to be inverted is $\alpha(a)$. Plate 1 shows $\alpha(a)$ for both space-based and airborne occultation geometries. The

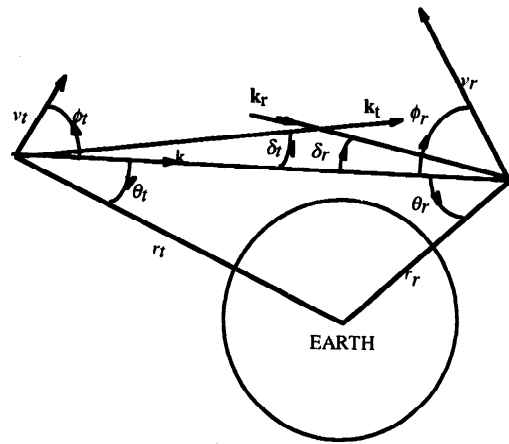


Figure 2. A pictorial view defining the variables for a GPS transmitter/receiver link.

particular features of this function for the two different geometries (receiver inside and outside the atmosphere) are discussed below.

2.1 Abel Inversion Scheme

The Abel inversion has been used extensively in seismic and astronomical inversions, as well as in inverting planetary and Earth occultation data [e.g., Fjeldbo et al., 1971; Kursinski et al., 1997]; therefore we describe it here very briefly and point out its limitations for the case of receivers inside the atmosphere. When the bending is determined, then equation (2) can be inverted with an Abelian transformation [e.g., Tricomi, 1977] to solve for n as

$$\ln(n(a)) = \frac{1}{\pi} \int_a^\infty \frac{\alpha(a')}{a' \sqrt{a'^2 - a^2}} da'. \quad (5)$$

Note that since the upper limit of the integral is infinity, it makes it necessary to have measurements of α starting from outside the atmosphere (where α vanishes) for this integral to be performed. When the receiver lies inside the atmosphere at radius r_r , then only measurements of $\alpha(a)$ for $a < r_r$ ($n(r_r)$) are available; therefore equation (5) cannot be applied and another approach must be used, which is presented in the following.

2.2. Ray-Tracing-Based Inversion Technique

2.2.1 Least squares estimation. At a high level, our technique can be described as a constrained least squares estimation. Since such formalism is well documented [Rodgers, 1976; Menke, 1989], we start with a short summary of its mathematical description to help the reader identify how the operators we are about to introduce fit into the general scheme and clarify our terminology. Let us first introduce the basic equations for a least squares estimation involving nonlinear operators; in this case, the linearization of the equation leads to an iterative scheme, outlined below

$$y = F(x) + \epsilon$$

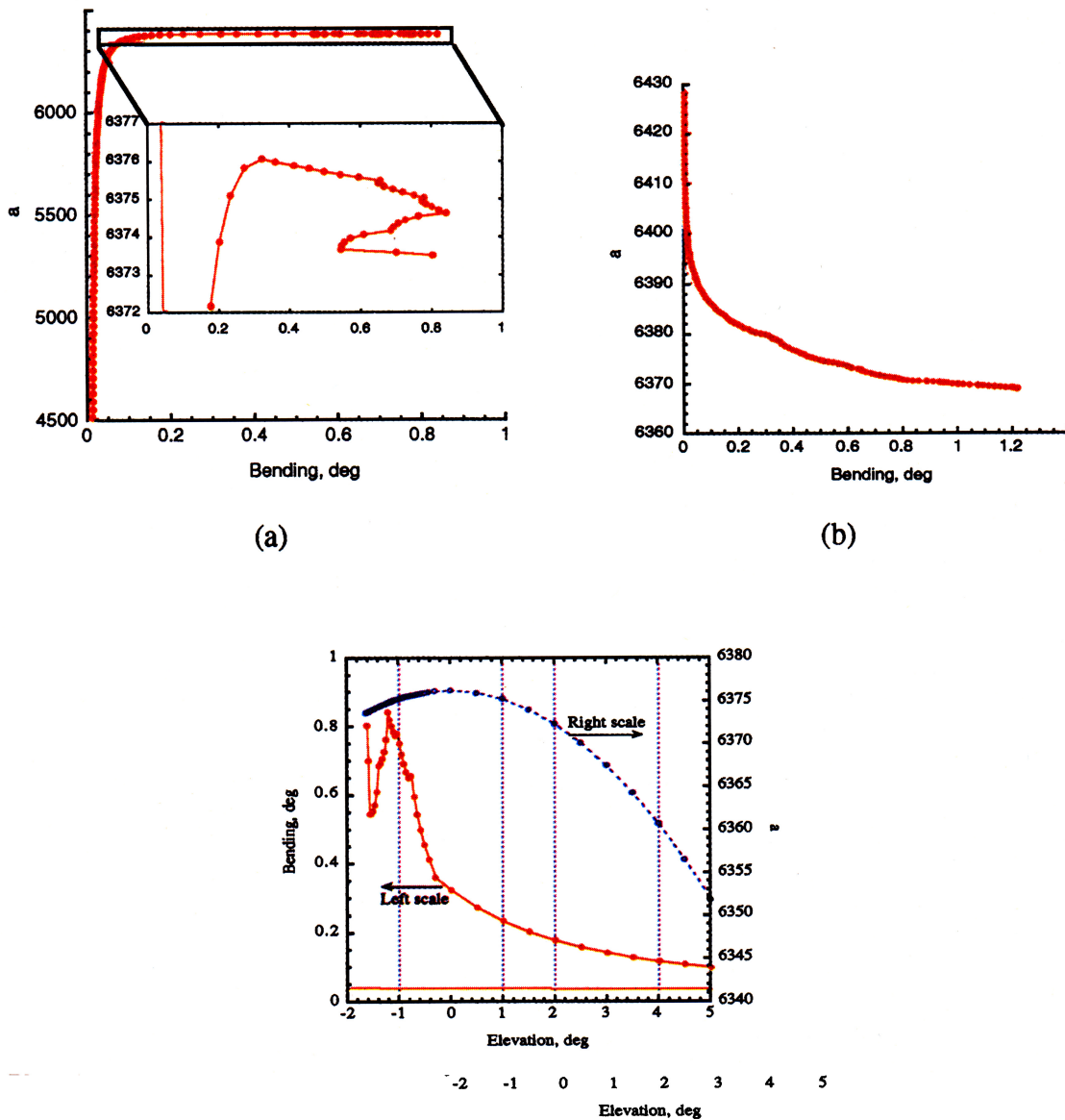


Plate 1. (a) Signal bending as a function of a (inverted scales) for a receiver inside the atmosphere (the inside plot is a magnification of the top portion of the plot); (b) bending versus a for a space-based occultation; (c) bending (left scale) and a (right scale) as a function of elevation for a receiver at 5 km altitude.

from which

$$y = y_n + K_n(x - x_n) + \epsilon, \tag{6}$$

where

$$y_n = F(x_n) \quad \text{and} \quad K_n = \left. \frac{\partial F(x)}{\partial x} \right|_{x=x_n}$$

In equation (6), y is the measurement vector, x is the state vector to be estimated, F is the model operator, in our case nonlinear, K_n is the model gradient introduced in the linearization of the problem, ϵ is the measurement error, and x_n is the approximation of the solution at the n th iteration step. When there are additional a priori constraints they can be expressed in the analogous general form

$$c = G(x) + \delta$$

from which

$$c = c_n + L(x - x_n) + \delta \tag{7}$$

where

$$c_n = G(x_n) \quad L = \frac{\partial G(x)}{\partial x} = \text{independent of } x,$$

where c is the constraint or “virtual measurement” vector, G is the constraint operator, L is the constraint gradient introduced in the linearization step, and δ is the virtual measurement uncertainty. We will show that for our particular problem, G is linear and therefore L does not depend on x . Note that in the particular case of $G(x)=x$, the operator L is reduced to the identity and the above equation reduces to $x=x_0$, which is referred to as a priori estimate. One can see that the a priori estimate is a special case of a priori constraint.

In a constrained least squares minimization, equations (6) and (7) are solved together, and a solution is sought to

minimize the error defined by

$$E_{y,c} = [y - y_n - K_n(x - x_n)]^T S_y^{-1} [y - y_n - K_n(x - x_n)] + [c - c_n - L(x - x_n)]^T S_c^{-1} [c - c_n - L(x - x_n)], \quad (8)$$

where $S_y = \langle \epsilon \epsilon^T \rangle$ is the measurement error covariance and $S_c = \langle \delta \delta^T \rangle$ is the constraint error covariance. The solution and estimate error covariance are given by

$$\hat{x} = x_n + [K_n^T S_y^{-1} K_n + L^T S_c^{-1} L]^{-1} [K_n^T S_y^{-1} (y - y_n) + L^T S_c^{-1} (c - c_n)] \quad (9)$$

$$S_{\hat{x}} = [K_n^T S_y^{-1} K_n + L^T S_c^{-1} L]^{-1}.$$

Note that the constraint equations are formally (mathematically) treated like the measurement equations, and this clarifies why they are referred to as “virtual measurements.”

2.2.1.1. Model and state vector. We choose to represent the atmosphere as a set of m_L concentric layers of specified thickness, with refractivity varying exponentially as a function of radius with a fixed scale height for each layer. This continuous exponential model is used in the numerical calculation of the integral in equation (2); such an integral corresponds to the nonlinear model F. The specific functional form for refractivity as a function of r , the radial distance from the Earth's center to a point in layer j , where $R_{j+1} > r > R_j$ is given by

$$N(r) = N_{norm} \exp\left(-\frac{r - R_j}{H_j}\right) \prod_{i=j}^{j_{norm}-1} \exp\left(+\frac{\Delta_i}{H_i}\right) j < j_{norm}, \quad (10a)$$

$$N(r) = N_{norm} \exp\left(-\frac{r - R_j}{H_j}\right) \prod_{i=j_{norm}}^{j-1} \exp\left(-\frac{\Delta_i}{H_i}\right) j > j_{norm}.$$

In general,

$$N(r) = N_{norm} \exp\left(-\frac{r - R_j}{H_j}\right) \prod_{i=\beta}^{\gamma} \exp\left(\delta \frac{\Delta_i}{H_i}\right) \text{ any } j \neq j_{norm}, \quad (10b)$$

$$N(r) = N_{norm} \exp\left(-\frac{r - R_j}{H_j}\right) j = j_{norm},$$

where R_j is the lower boundary of the j th layer, Δ_i and H_i are the i th layer thickness and scale height. Note that the meaning of δ , β , and γ is obtained by inspection of equation (10). In equation (10) we introduce one additional parameter, the normalization factor of refractivity, N_{norm} , which is taken to be the value at the lower boundary of a designated normalization layer j_{norm} . Our “state vector” is therefore composed of a set of scale heights and a normalization value of refractivity. Initial values of N_{norm} and H_i values are obtained with a procedure discussed later.

2.2.1.2. Measurement vector and constraint equations. The “measurement vector” is composed of a set of m_p positive and m_n negative elevation bending data. Since each bending measurement at negative elevation is heavily weighted by the atmospheric structure at the layer where the tangent point resides, the atmospheric structure below the height of the receiver is expected to be strongly

constrained by the bending measurements. Indeed, we will demonstrate that refractivity can be uniquely retrieved up to the height of the receiver without the help of other information. However, as we start going to higher elevation, data become strongly correlated, and we must rely on other a priori information to be able to obtain a unique solution for the atmosphere at high altitudes. In our work we introduce m_r refractivities taken from an atmospheric model (referred to as a priori model) above the receiver. They are “virtual measurements” added as constraint equations.

The inversion consists of finding the optimal set of scale heights and an overall normalization factor that best fit the measured bending angles and a priori constraints, weighted by their respective measurement uncertainty. In the following sections we give a detailed description of the specific formulation of our problem, consistent with the formalism outlined above.

2.2.2 Data Smoothing and Atmospheric Layering.

When the receiver is outside the atmosphere, bending measurements are smoothed over the time it takes the tangent height of the ray to descend the diameter of the first Fresnel zone [Kursinski *et al.*, 1997]. In the geometrical optics framework these smoothed measurements can be considered independent. When the receiver is inside the atmosphere, we group the bending measurements α_i into a set of negative elevation measurements and a set of positive elevation measurements (Figure 1). Distinguishing between positive and negative elevation is possible based on a basic property of the form of the function $\alpha(a)$. The typical behavior of $\alpha(a)$, when the receiver is inside the atmosphere, is illustrated in Plate 1a, contrasted with that obtained for a receiver in space, shown in Plate 1b. While the latter does not have a local maximum or minimum, the former has a maximum exactly at the point that separates positive and negative elevation measurements (as seen from Plate 1c). This general property about a stationary receiver inside the atmosphere follows from equation (1), which implies that a is maximum when the signal is received at zero elevation, since $n(r_R) r_R$ (r_R is the radius of the receiver in this case) is constant. When the receiver is moving inside the atmosphere, separating positive and negative elevation data can be more difficult, depending on the dynamics of the motion. However, in most practical situations the motion will be slow enough such that a similar, although more complicated, treatment is possible.

Smoothing of negative elevation data is treated in the same way as space-based measurements in the manner just described. In contrast, the contribution to bending for positive elevation data is far more evenly distributed along the path, so positive elevation measurements become strongly correlated as the elevation rises a few degrees above zero. Therefore smoothing time for the positive elevation data is not so well defined as that for the negative elevation data. Temporal smoothing of positive elevation data is then chosen such that data points are obtained at specified elevations. In general, it is expected that because of their diminishing strength, those measurements

corresponding to the first few degrees above the horizon will play the most important role in retrieving the refractivity above the receiver.

On an initial guess at the solution, approximate values for $r=a/n$ corresponding to the original negative elevation bending measurements are determined. Layer boundaries are then introduced between each pair of r values; the number of layers below the receiver then corresponds to the number of independent measurements (negative elevation bending) and their thickness is limited by the Fresnel zone size. The thickness of the layers immediately above the receiver (by 1-2 km) is chosen to be commensurate to those below the receiver; as we move higher, the thickness of the layers is chosen to be consistent with the resolution of the chosen a priori atmospheric model, or of other types of measurements (e.g., radiosonde) if available.

2.2.3 Inversion Scheme. It was stated that equation (10) represents our mathematical model for atmospheric refractivity, while our model for bending is given by the integral in equation (2), evaluated numerically with refractive index obtained from our refractivity model. Values of the state vector $\{H_i, N_{norm}\}$ can then be solved for, in a least squares sense, to fit the m_n+m_p measurements of bending and the complementary m_r values of N . Because the problem is severely nonlinear, it is advantageous to mitigate the nonlinearity by working with the logarithm of the refractivity given by

$$\ln(N(r)) = \ln(N_{norm}) + \delta \frac{r - R_j}{H_j} - \sum_{i=\beta}^{\gamma} \frac{\Delta_i}{H_i} \quad (11)$$

and change the state vector to $\{1/H_i, \ln(N_{norm})\}$. The reader can now identify the terms of equation (11) with those of equation (7).

Similarly, the nonlinearity of equation (2) is reduced by working with the logarithm of the bending. However, since the reformulated problem is not completely linear, a few iterations are required before a solution is reached. At each iteration k , we use the set of parameter values $\{1/H_i^k, \ln(N_{norm}^k)\}$, equation (11) and the discretized form of equation (2) to calculate the bending and refractivity. The integration in equation (2) is performed numerically, using the values $\{1/H_i^k, \ln(N_{norm}^k)\}$ in each layer to calculate the index of refraction n . For each negative elevation bending measurement, the radius of the tangent height r_{min} is then estimated knowing a ; such radius is the lower integration boundary for tracing the ray from the transmitter to the receiver. (For positive elevation bending the lower integration boundary is the receiver position.) Evolution of the solution from one iteration to the next is accomplished by Taylor expanding around $\{1/H_i^k, \ln(N_{norm}^k)\}$ and introducing the partial derivatives of the logarithm of bending and refractivity with respect to the state vector. Note that the derivatives of the bending measurements are calculated numerically and vary at each iteration. By contrast, the partial derivatives of the logarithm of the refractivity are easily calculated

analytically from equation (11). The calculation is done only once since the operator is linear and hence they do not vary with $\{1/H_i^k, \ln(N_{norm}^k)\}$. To first order, this can be expressed as

$$\ln(\alpha_m) = \ln(\alpha_c(p)) + \sum \frac{\partial}{\partial p} \ln(\alpha_c(p)) \Delta p, \quad (12a)$$

$$\ln(N_m) = \ln(N_c(p)) + \sum \frac{\partial}{\partial p} \ln(N_c(p)) \Delta p,$$

where

$$p = \{1/H_i^k, \ln(N_{norm}^k)\} \quad (12b)$$

$$\{1/H_i^{k+1}, \ln(N_{norm}^{k+1})\} = \Delta p + \{1/H_i^k, \ln(N_{norm}^k)\}.$$

In the previous equation we used the subscript c to indicate computed quantities. The solution is thus obtained for the vector of parameter variations Δp , from which the new estimate is recovered as shown in line 2 of equation (12b). Note that the first line in equation (12a) corresponds to equation (6), whereas the second line corresponds to equation (7); the linearized operators K_n and L can be identified with the gradients of the logarithm of bending and refractivity, respectively. Moreover, $\{1/H_i^k, \ln(N_{norm}^k)\}$ can be identified with x_n of equation (9) and $\{1/H_i^{k+1}, \ln(N_{norm}^{k+1})\}$ can be identified with \hat{x} of equation (9). Regarding the estimate error covariance, it is first noted that each measurement has an associated error, which is used to weight the corresponding equation in the solution process. Throughout this work the error in the refractivity N obtained from the a priori model is assumed to have a Gaussian distribution with $\sigma_N = 0.05N$. This is a conservative estimate for regions above the receiver height. However, the objective of our investigation is that of assessing the strength of bending data per se in the retrieval of refractivity. To isolate the roles of bending angles and refractivities in the retrieval accuracy, the a priori constraints are intended to be used only above the receiver heights. Moreover, the height above the receiver at which constraints are added are also varied in our simulations. This way, if convergence to the truth is reached, it is unambiguous to attribute the result to the strength of the bending data. For the bending measurements we have estimated $\sigma_\alpha = 0.01\alpha + 10^{-5}$ (radians). This value comprises the error due to the spherical symmetry approximation (first addendum, dominant at low altitudes) and to the receiver thermal noise (second addendum, dominant at high altitudes). This error is somewhat conservative for the positive elevation-bending measurements for a fixed receiver. For an airborne receiver the noise appearing on the phase would be primarily due to multipath and airplane rough motion. On the basis of examination of postfit residual data from airplane the estimation of Fresnel zone sizes and the velocity of descent of the link, we estimate that the error given above applies also to the case of an airborne receiver. In the present analysis a diagonal covariance is assumed for both bending and refractivity, and in the notation of equation (8) and (9), $S_y = \langle \sigma_\alpha \sigma_\alpha^T \rangle$ and S_c

$= \langle \sigma_N \sigma_N^T \rangle$. Because of this assumption, the σ associated with each measurement is simply used to normalize the corresponding equation in the retrieval process [Rodgers, 1976]. The above terms form the error covariance S_x of equation (9).

At each new iteration, the tangent point radius r_{min} , associated with a given impact parameter a is obtained by recursively solving $a(r_{min}) = n(r_{min}) \times r_{min}$ using the latest solution. Knowledge of r_{min} is needed to recompute the bending measurements (equation (2)) and the partials (first line in equation (12a)). Even though the r_{min} values can change as we iterate, the boundaries of the layers are fixed, and they are based on the initial layering scheme outlined above.

2.2.4. Obtaining a first estimate. A first-guess state vector based on the a priori model or climatology data can be quite inaccurate at altitudes within a few kilometers of the surface. The reason is associated with the abundance and variability of water vapor in the lower troposphere and particularly its vertical variations, which can be estimated quite poorly in weather analyses. Because of the nonlinear relationship between the state vector and the bending angles, a poor initial guess can slow down or even prevent convergence in the retrieval process. Our solution is to derive a much better first guess, particularly near the surface, using the bending angle measurements directly.

A general property of the function $\alpha(a)$ for a fixed receiver inside the atmosphere is that for every negative elevation measurement, there corresponds a positive elevation measurement with the same value of a (as seen from Plate 1c). Moreover, because of the spherical symmetry assumption, one can observe that the sum of the negative and positive elevation data pair corresponding to a given a is equal to the bending that would be obtained with a receiver outside the atmosphere for that same a . Hence we can construct the “space-based equivalent” $\alpha(a)$ profile for $a < n(r_R)r_R$. Next, to extend the values of $\alpha(a)$ and a to higher altitudes, we construct $\alpha(a)$ for $a > n(r_R)r_R$ using the same atmospheric model introduced for the a priori constraints. We compute α from equation (2) for a distribution of asymptote miss distances, therefore obtaining the bending that would have been observed from space for the assumed a priori model. The complete $\alpha(a)$ profile thus obtained can be inverted using equation (5) to obtain a first-guess refractivity profile. A first estimate for the state

vector, to be used in the inversion scheme, is simply obtained from this profile from equation (10).

By construction, the resulting first-guess refractivity profile will have exactly the same structure as the a priori atmospheric model above the receiver but can have substantially different structure below the receiver, where the profile is largely driven by the data.

3. Numerical Results

3.1. Receiver Outside the Atmosphere

The first step in the validation of our technique consists of reproducing some refractivity profiles that have been previously derived with the Abel approach. We used data obtained from GPS/MET. We illustrate the comparisons in Plate 2 for one particular occultation occurred in May 1995 at the approximate location (69° N, -83° W).

For both inversion techniques the fractional refractivity difference between GPS/MET and the ECMWF (European Centre for Medium-Range Weather Forecasting) or NCEP (National Center’s for Environmental Prediction) models are shown. Note that except at very high altitudes the Abel and ray-tracing techniques reproduce nearly identical retrievals with differences in absolute value $< (0.1-0.5\%)$. The larger differences occur near sharp changes in refractivity, where the ray-tracing routine appears to produce a somewhat smoother retrieval than the Abel inversion. At altitudes above 40 km, differences of about 1-5% are observed (Plate 2b) between the Abel and the ray-tracing inversions.

When refractivity is obtained, then temperature profiles in dry regions (upper troposphere and stratosphere) can be derived from the ideal gas law and hydrostatic equilibrium [Kursinski *et al.*, 1997]. In the lower and midtroposphere, independent information of temperature can be used to derive accurate water vapor from refractivity [Kursinski and Hajj, 1998]. In general, the refractivity information with associated covariance will be combined with independent information from an analysis (or something equivalent) with a corresponding covariance to derive optimal estimates of temperature and water vapor.

Temperature differences between the NCEP model and the Abel and ray-tracing inversions are shown in Plate 2c, where water vapor in the lower troposphere is assumed to be that of the NCEP. An initial value of temperature was needed in order to represent the mass above 50 km in the hydrostatic equilibrium integral, and it was taken to be that of the NCEP at 50 km, which explains the exact agreement of the retrievals and the model at that height. It was established elsewhere [e.g., Kursinski *et al.*, 1996; Ware *et al.*, 1996] that temperature accuracy of GPS/MET is < 2 K between 5 and 25 km. Larger T differences within these heights in Plate 2 are reflective of errors in the NCEP model. At altitudes higher than 30 km (~ 10 mbar), Plate 2 shows that our inversion agrees with NCEP to better than 5 K.

Table 1. Set of Locations Chosen to Retrieve Refractivity With Receiver at 5 km

Case	Latitude(°)	Longitude(°)
1	40	180
2	34	-120
3	20	-160
4	-10	40

3.2. Receiver Inside the Atmosphere

The situation where a receiver is within the atmosphere was simulated by constructing an artificial occultation, with a fixed receiver at 5 km altitude tracking the GPS at both positive and negative elevations. Taking a refractivity profile interpolated from ECMWF analysis at a specified location to be the truth, a set of rays linking the transmitter to the receiver were constructed with specified tangent heights, ranging from the surface up to the receiver's height. Similarly, a set of rays linking the transmitter to the receiver were constructed to correspond to positive elevation angles above the receiver horizon and having impact parameter given by equation (1), where r is the radius of the receiver and ϕ is between 90° (0° elevation) and 180° (zenith). Noise was added to the simulated bending measurements with $\sigma_\alpha = 0.01\alpha + 10^{-5}$ (radians), as discussed in Section 3.1. Additional constraints or "virtual measurements" of refractivity above the receiver location were taken from the NCEP model. The NCEP analyses used here are the global stratospheric analyses. As such, their representation of the troposphere can differ markedly from the ECMWF analyses at the same location, providing a good test of the ability of the bending measurements to retrieve the "true" profile. All measurements were normalized to their respective σ , as discussed in Section 2.2.4, to establish their relative weight in the inversion process.

Four different geographical locations for the receiver were considered, two at midlatitudes and two in tropical regions, as illustrated in Table 1. The "true" profiles of temperature and water vapor partial pressure (obtained from the ECMWF analyses) used to generate the synthetic data set are shown in Plate 3. The first guess at the solution for refractivity was generated with the procedure described in Section 2.2.3, and the relative error with respect to the truth is illustrated in Plate 4 for the four cases examined here. In essence, by making use of the bending data, complemented by other information above the receiver, a reasonable initial guess of the model state vector can be obtained, particularly at low elevation. Although there are other ways for choosing a first guess at the solution, the one introduced here has the advantage that it makes use of information contained in the bending measurements. As a result, the robustness of the inversion algorithm is increased because smaller parameter variations are required. At the same time fewer iterations are necessary to converge.

An example of a synthetic data set of $\alpha(a)$ generated for case 4 (see Table 1) is shown in Plate 1a. The top of Plate 1a is magnified in order to illustrate some of the potentially complicated structure of this curve associated with atmospheric multipath, which occurs when the signal travels along more than one path due to some sharp layers in the atmosphere. In particular, the $\alpha(a)$ structure of Plate 1a shows that as the signal descends below 5 km, at some point it branches into three distinct signals coming from three different heights in the atmosphere, as described in the occultation of the Uranus atmosphere by Lindal *et al.*

[1987]. This branching coincides with a very sharp layer of water vapor at about 3 km, as illustrated in Plates 3 and 4 (case 4). The branching of the signal can be explained as follows. Before the signal reaches the top of the layer, there is only one ray in the atmosphere (ray 1). As ray 1 reaches the top of the layer, a second signal appears simultaneously from the bottom of the layer and it branches into two signals, one moving upward (ray 2) and one moving downward (ray 3). Rays 1 and 2 merge together nearly at the peak of the layer, while ray 3 continues to go down into the atmosphere. Under certain conditions, the atmospheric inversion layer can block the signal for some time, giving a very clear indication of the height of the trade wind inversion [Hajj *et al.*, 1994].

To assess the merits of the inversion technique for the different cases, several numerical tests were performed to simulate possible strategies of complementing bending measurements with refractivity and to understand their impact on retrievals. In the first test we assumed that the refractivity from NCEP was specified directly above the receiver location and up to heights of about 60 km. Above 60 km the refractivity was extrapolated assuming an isothermal atmosphere. For this situation we quantified the effect of positive elevation bending measurements on the retrieval accuracy. The results are presented in Plates 5 and 6 for the cases of excluded and included positive elevation bending, respectively. When positive elevation bending measurements were included, only angles up to 30° above the horizon were used because measurements at higher elevation were believed to have no strength in resolving the vertical structure.

In all cases we present the fractional error in the retrieved refractivity with respect to the "truth" (ECMWF) and, additionally, the fractional error of the a priori refractivity (NCEP) with respect to the truth. Plate 5 shows that the retrieval error is small close to the ground and increases as the receiver height is approached, consistently with the expectation that at heights above the receiver the solution be given by the NCEP analysis, the constraint. The addition of positive elevation bending measurements causes noticeable reduction of the retrieval error, suggesting that they have sufficient strength to improve the inversion below and around the receiver location. Above the receiver height, the solution transitions between the truth to the NCEP in the space of 1-2 km. It is noted that all bending measurements are weighted more than the refractivities by the retrieval algorithm; in spite of this our results show that above the receiver height the solution does not deviate noticeably from the a priori values in all cases, indicating that the precise choice of the σ for the refractivities is not crucial. The relatively rapid shift of the solution to the a priori constraint profile indicates that the positive elevation-bending angles place relatively little constraint on the vertical refractivity structure above the altitude of the receiver.

To further understand the role of positive elevation-bending measurements in retrieving refractivity profiles

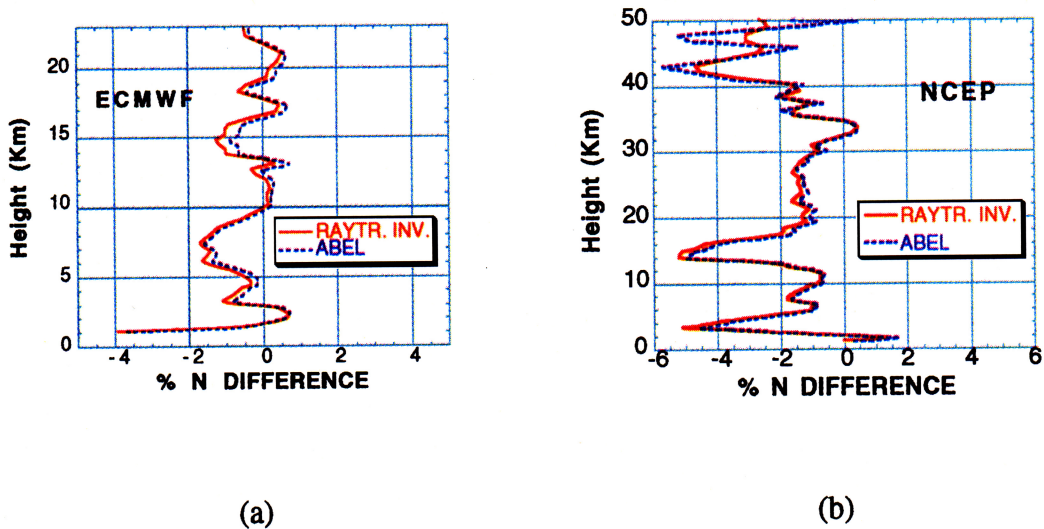


Plate 2. (a) Fractional refractivity difference between ECMWF model and GPS/MET data inverted with the Abel and ray-tracing techniques; (b) same as in Plate 2a but for the NCEP model; (c) same as Plate 2b but for temperature.

above the receiver location, we performed a second numerical test where we removed refractivity data at heights below 25 km, to simulate a case where the available model is known to be inaccurate and little weight is placed on the virtual measurements. The results are illustrated in Plate 7 for the four cases of Table 1, which shows that the retrieval accuracy below the receiver is the same as that of Plate 6. This is an indication that the bending alone is driving the retrieval process at all heights below the receiver height and up to 1 km above it in some cases. On the other hand, the error above the receiver location increases appreciably. Evidently, the noise present on the positive elevation-bending measurements renders them unable to resolve the profile at high altitudes.

4. Conclusions

We have described and demonstrated a technique appropriate for inverting GPS occultation data, obtained from a location within the atmosphere, to retrieve vertical profiles of refractivity. This technique could also be extended to the assimilation of bending angle data into numerical weather models. Close agreement with the Abel results, in the applicable cases, confirms the correctness of the approach and implementation. Results presented for the simulated case of a receiver fixed at 5 km indicate accuracy better than 0.5% for the refractivity retrieved below the receiver, when positive elevation bending data are included. Additionally, the results show that the retrieved vertical

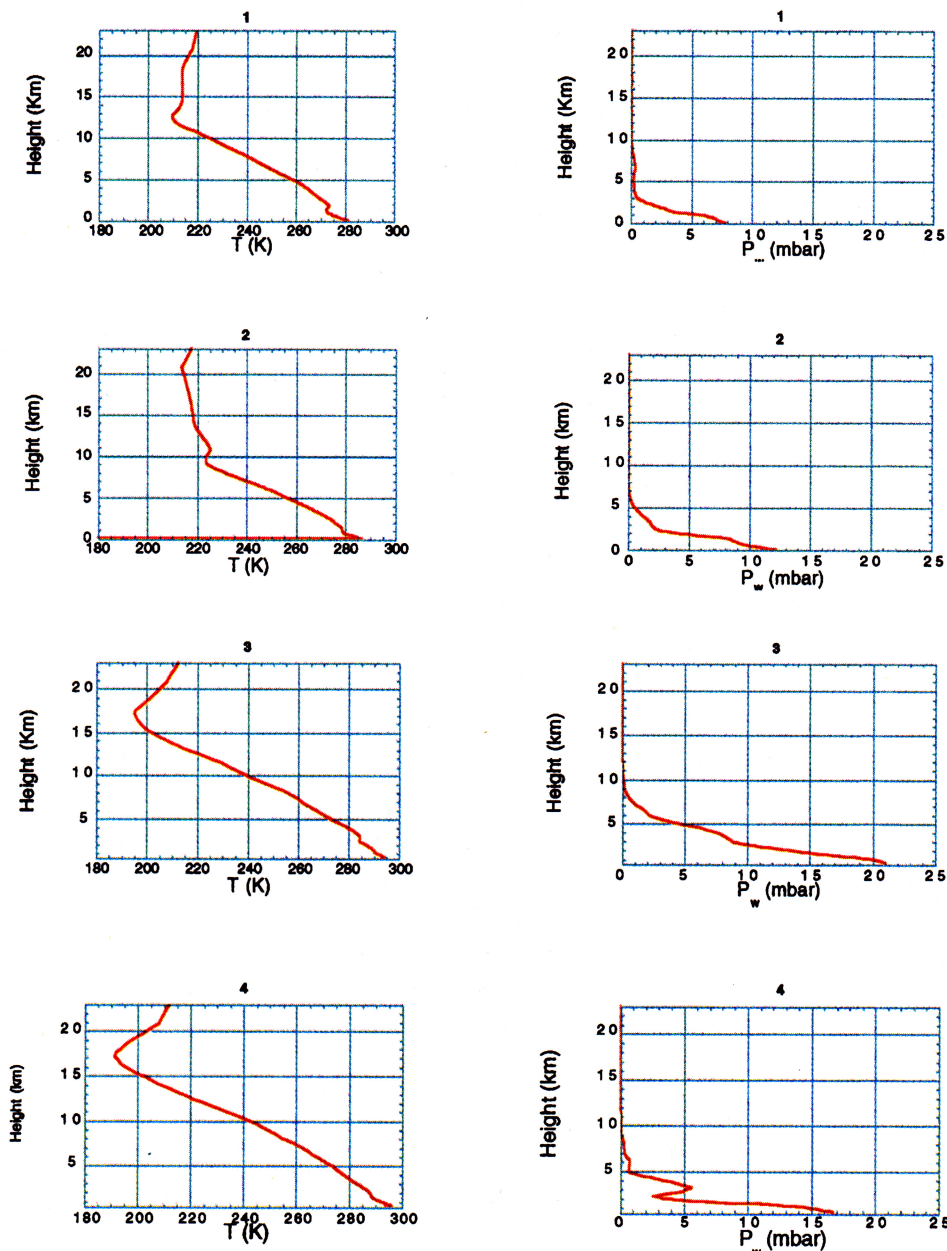


Figure 5. Temperature (left) and water vapor partial pressure (right) obtained from ECMWF at the four locations of Table 1.

refractivity structure at all heights up to about 1 km above the receiver altitude does not depend on the accuracy of the a priori model values introduced above the receiver; indeed, it does not require them.

Therefore if a vantage point located a few kilometers above the surface can be provided for GPS receivers such as on a mountain, or an airplane, the technique described here offers a simple method of obtaining vertical information on the lower atmosphere up to the receiver altitude. About one hundred measurements per day per receiver could be obtained in a given region, in contrast to radiosondes that are launched once or twice daily. Since vertical information is extremely important in characterizing the stability of the atmosphere and is expensive to acquire, the profiles obtainable from limb and down looking GPS receivers may prove quite useful for applications such as regional weather

forecasting, hydrology, surface-air exchange, and related topics of atmospheric research.

Although the conclusions drawn above are based on the examination of synthetically generated bending data, we are encouraged by our very promising preliminary results and plan to pursue a validation effort using real data in the near future. Finally, it is important to note that even though we have validated this technique assuming a layered exponential model for the atmosphere, the approach can easily be generalized to include some horizontal variation of the gradient of refractivity.

Acknowledgments. This work has been performed at the Jet Propulsion Laboratory, Pasadena, under contract with the National Aeronautical and Space Administration. The research was supported by the NASA Office of Earth Science.

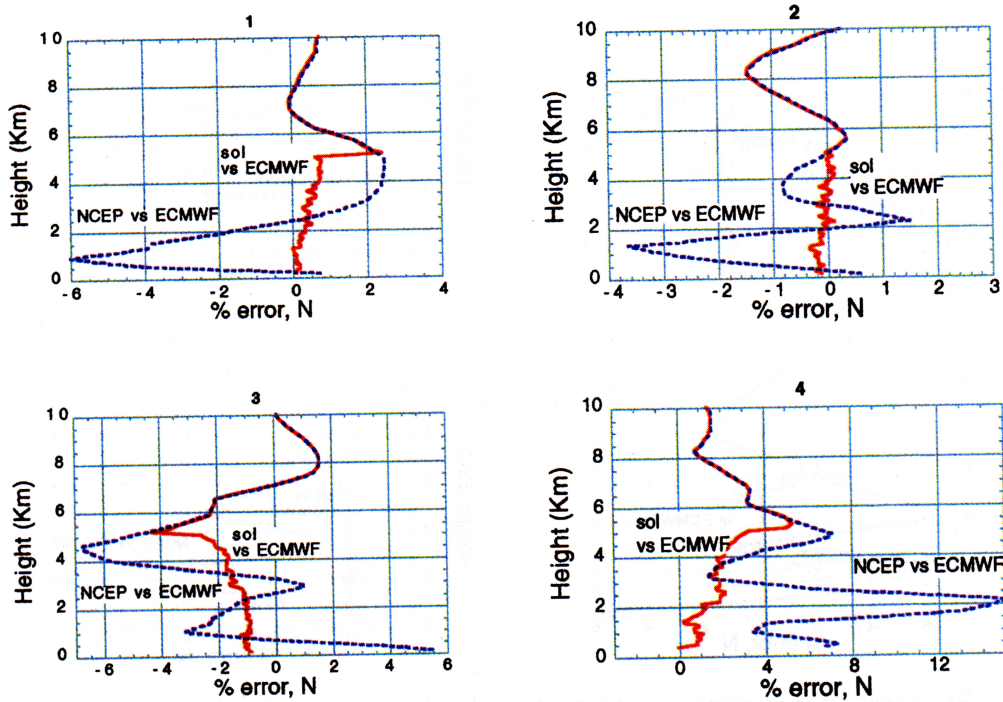


Plate 4. Fractional error in refractivity used as first guess at the solution, before retrieval.

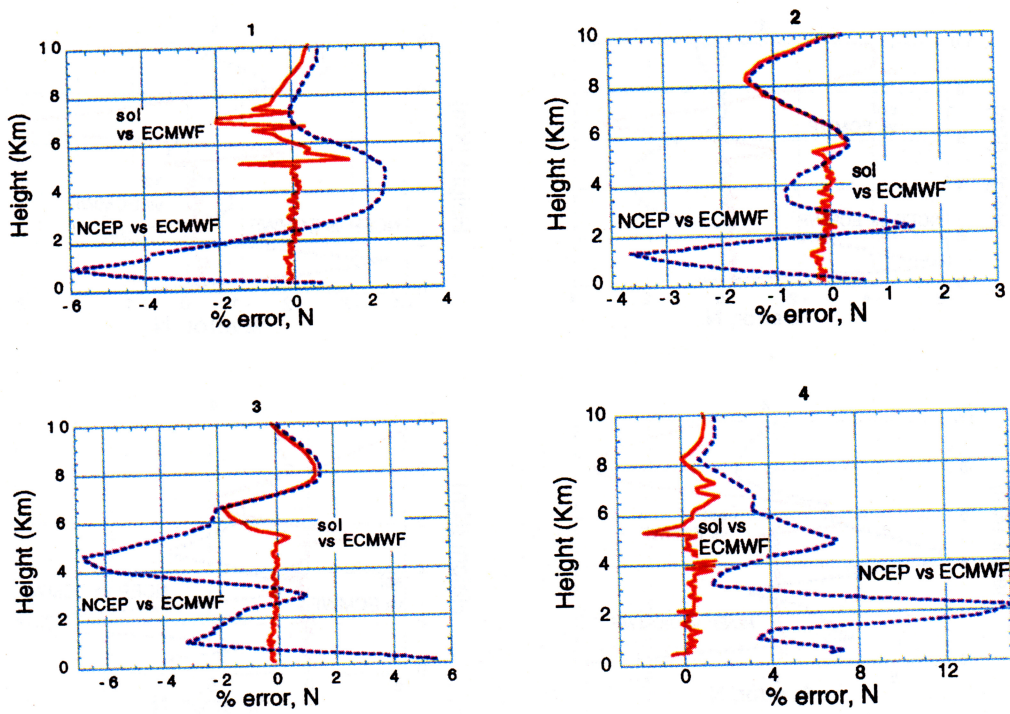


Plate 5. Fractional error in retrieved refractivity (sol) when positive elevation measurements are not included.

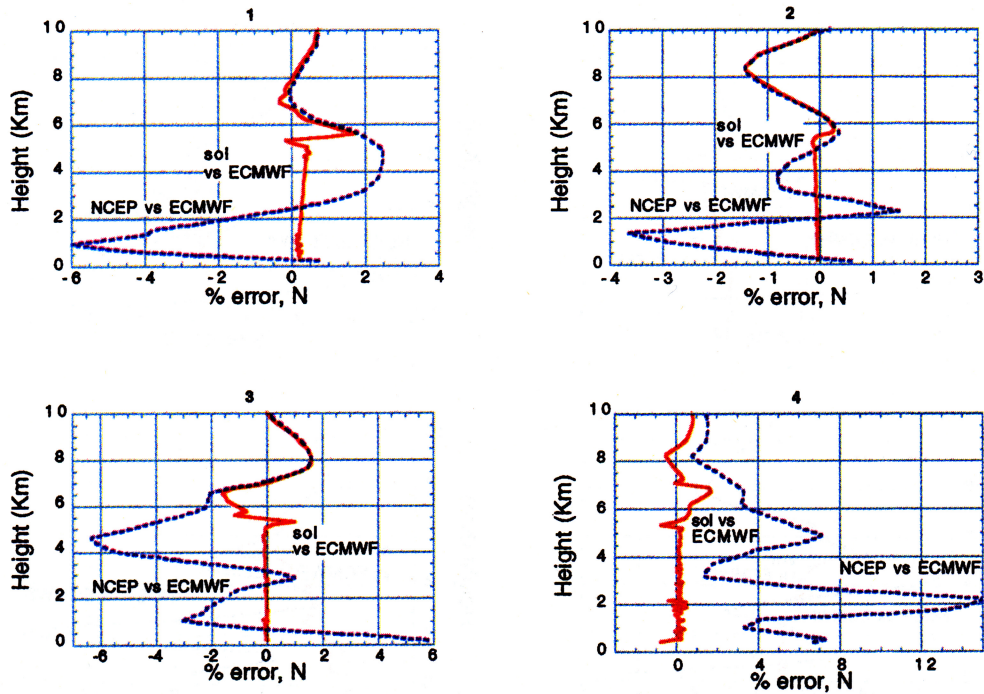


Plate 6. Fractional error in retrieved refractivity (sol) when positive elevation measurements are included.

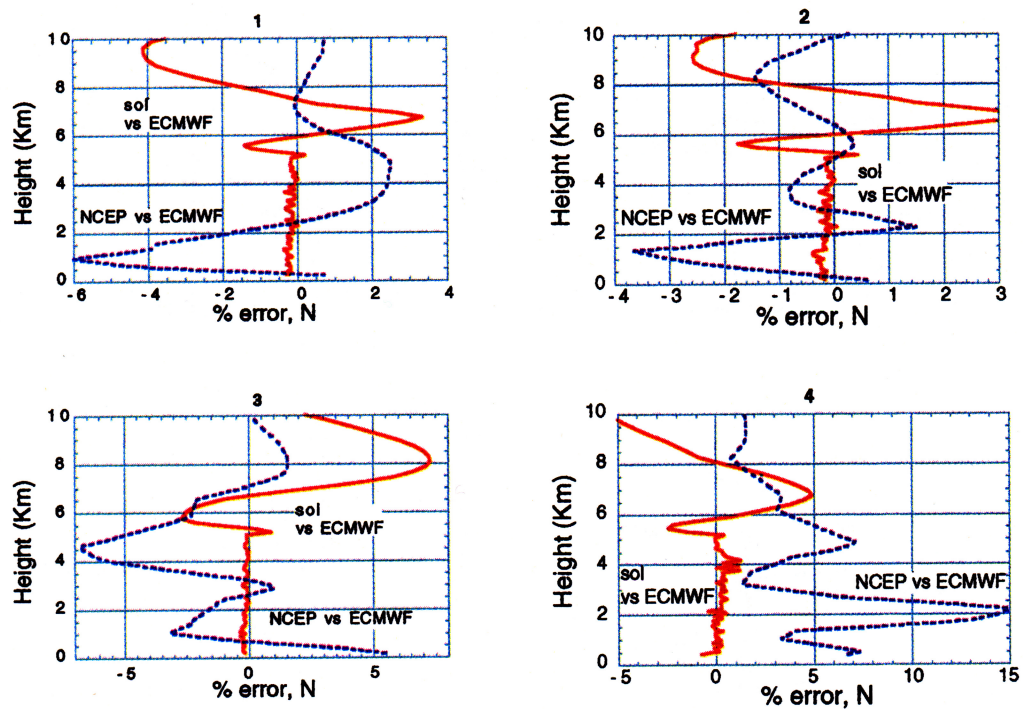


Plate 7. Fractional error in retrieved refractivity (sol) when positive elevation measurements are included and no refractivity below 25 km is used.

References

- Born, M., and E. Wolf, Principles of Optics, 122 pp., 6th ed., Pergamon, New York, 1980.
- Eyre, J.R., Assimilation of radio occultation measurements into a numerical weather prediction system, *Tech. Memo 199*, Eur. Cent. for Medium-Range Weather Forecasts, Reading, England, 1994.
- Fjeldbo, G., A. J. Kliore, and V. R. Eshleman, The neutral atmosphere of Venus as studied with the Mariner V radio occultation experiments, *Astron. J.*, 76, 123-140, 1971.
- Gorbunov, M.E., S.V. Sokolovsky, and L. Bengtsson, Space refractive tomography of the atmosphere: Modeling of direct and inverse problems, *Tech. Rep. n° 210*, Max-Planck-Inst. fur Meteorol., Hamburg, Germany, 1996.
- Hajj, G.A., E.R. Kursinski, W.I. Bertiger, and L.J. Romans, Assessment of GPS occultations for atmospheric profiling, paper presented at the Seventh Conference on Satellite Meteorology and Oceanography, *Am. Meteor. Soc.*, Monterey, Calif., June 6-10, 1994.
- Hajj, G.A., E.R. Kursinski, W.I. Bertiger, S.S. Leroy, T. Meehan, L.J. Romans, and J.T. Schofield, Initial results of GPS-LEO occultation measurements of Earth's atmosphere obtained with the GPS/MET experiment, in *Proceedings of the Symposium on GPS Trends in Precise Terrestrial, Airborne, and Spaceborne Applications*, Springer-Verlag, New York, 1996.
- Kuo, Y.-H., X. Zou, Y.-R. Guo, Variational assimilation of precipitable water using a nonhydrostatic mesoscale adjoint model, moisture retrieval and sensitivity experiments, *Mon. Weather Rev.*, 124, 122-147, 1996.
- Kuo, Y.-H., X. Zou, W. Huang, The impact of global positioning system data on the prediction of an extratropical cyclone — An observing system simulation experiment, *J. Dyn. Atmos. Ocean*, 27(1-4), 439-470, 1998.
- Kursinski, E.R., and G. Hajj, An examination of water vapor derived from Global Positioning System occultation observations during June-July 1995, Zonal means, *J. Geophys. Res.*, in press, 1998.
- Kursinski, E.R., G.A. Hajj, K.R. Hardy, L.J. Romans, and J.T. Schofield, Observing tropospheric water vapor by radio occultation using the Global Positioning System, *Geophys. Res. Lett.*, 22, 2365-2368, 1995.
- Kursinski, E.R., et al., Initial results of radio occultation observations of Earth's atmosphere using the Global Positioning System, *Science*, 271, 1107-1110, 1996.
- Kursinski, E.R., G.A. Hajj, K.R. Hardy, J.T. Schofield, and R. Linfield, Observing Earth's atmosphere with radio occultation measurements, *J. Geophys. Res.*, 102, 23,429-23,465, 1997.
- Leroy, S.S., Measurement of geopotential heights by GPS radio occultation, *J. Geophys. Res.*, 102, 6971-6986, 1997.
- Leroy, S.S., Detecting climate signals: Some Bayesian aspects, *J. Clim.*, in press, 1998.
- Lindal, G.F., J.R. Lyons, D.N. Sweetnam, V.R. Eshleman, D.P. Hinson and G.L. Tyler, The atmosphere of Uranus: results of radio occultation measurements with Voyager 2, *J. Geophys. Res.*, 92, 14,987-15,001, 1987.
- Menke, W., *Geophysical Data Analysis: Discrete Inverse Theory*, Academic, San Diego, 1989.
- Rocken, C., et al., Analysis and validation of GPS/MET data in the neutral atmosphere, *J. Geophys. Res.*, 102, 29,849-29,866, 1997.
- Rodgers, C.D., Retrieval of atmospheric temperature and composition from remote measurements of thermal radiation, *Rev. Geophys.*, 14, 609-624, 1976.
- Tricomi, F.G., *Integral Equations*, Dover, Mineola, New York, 1977.
- Ware, R., et al., GPS sounding of the atmosphere from low Earth orbit — Preliminary results, *Bull. Am. Meteorol. Soc.*, 77, 19-40, 1996.
- Yuan, L.L., R.A. Anthes, R.H. Ware, C. Rocken, W.D. Bonner, M.G. Bevis, and S. Businger, Sensing climate change using the global positioning system, *J. Geophys. Res.*, 98, 14,925-14,937, 1993.
- Zou, X., Y.-H. Kuo, and Y.-R. Guo, Assimilation of atmospheric radio refractivity using a nonhydrostatic adjoint model, *Mon. Weather Rev.*, 123, 2229-2249, 1995.
- Zou, X., F. Vandenberghe, B. Wang, M. E. Gorbunov, Y.-H. Kuo, S. Sokolovskiy, J.C. Chang, and J.G. Sela, Direct assimilation of GPS/MET refraction angle measurements, 1, Concept and results of ray-tracing, 2, Variational assimilation using adjoint techniques *J. Geophys. Res.*, in press, 1998.

G.A. Hajj, E.R. Kursinski, and C. Zuffada, Jet Propulsion Lab., MS 238-600, 4800 Oak Grove Dr., Pasadena, CA 91109. (cinzia@cobra.jpl.nasa.gov)

(Received March 29, 1999; revised July 8, 1999; accepted July 16, 1999.)